NRC Research Press

ARTICLE

Magnetic surveying with an unmanned ground vehicle

A. Hay, C. Samson, L. Tuck, and A. Ellery

Abstract: With the recent proliferation of unmanned aerial vehicles for geophysical surveying, a novel opportunity exists to develop unmanned ground vehicles in parallel. This contribution features a study to integrate the Husky A200 robotic development platform with a GSMP 35U magnetometer that has recently been developed for the unmanned aerial vehicle market. Methods to identify and reduce the impact of magnetically noisy components on the unmanned ground vehicle platforms are discussed. The noise generated by the platform in laboratory and gentle field conditions, estimated using the fourth difference method for a magnetometer–vehicle separation distance of 121 cm and rotation of the chassis wheels at full speed (1 m/s), is ±1.97 nT. The integrated unmanned ground vehicle was used to conduct two robotic magnetic surveys to map cultural targets and natural variations of the magnetic field. In realistic field conditions, at a full speed of 1 m/s, the unmanned ground vehicle measured total magnetic intensity over a range of 1730 nT at 0.1 m spatial resolution with a productivity of 2651 line metres per hour.

Key words: geophysical magnetic method, magnetic interference, unmanned ground vehicle, fourth difference noise profile, robotic surveying.

Résumé : Avec la récente prolifération de véhicules aériens sans pilote utilisés pour faire des levés géophysiques, une nouvelle occasion existe pour développer des véhicules terrestres sans pilote en parallèle. Cette contribution présente une étude pour intégrer la plate-forme de développement robotisée Husky A200 munie d'un magnétomètre GSMP 35U qui a récemment été développé pour le marché des véhicules aériens sans pilote. Des méthodes pour identifier et réduire l'impact de composants magnétiquement bruyants sur les plates-formes de véhicule terrestres sans pilote sont discutées. Le bruit produit par la plate-forme dans des conditions de laboratoire et modérées de terrain, estimé en employant la méthode de quatrième différence pour une distance de séparation entre le véhicule et le magnétomètre de 121 cm et la rotation des roues de châssis à pleine vitesse (1 m/s), est ± 1,97 nT. Le véhicule terrestre sans pilote intégré a été utilisé pour effectuer deux levés magnétiques robotisés afin d'établir la carte de cibles culturelles et les variations naturelles du champ magnétique. Lors d'essais en conditions de terrain réalistes, effectués à pleine vitesse de 1 m/s, le véhicule terrestre sans pilote a mesuré l'intensité magnétique totale sur une gamme de 1730 nT à résolution spatiale de 0,1 m avec une productivité de 2651 mètres linéaires par heure. [Traduit par la Rédaction]

Mots-clés : méthode magnétique en géophysique, interférence magnétique, véhicule terrestre sans pilote, profil de bruit par quatrième différence, levé robotisé.

Received 23 April 2018. Accepted 28 August 2018.

A. Hay and L. Tuck. Department of Earth Sciences, Carleton University, Ottawa, ON K1S 5B6, Canada.
C. Samson. Department of Earth Sciences, Carleton University, Ottawa, ON K1S 5B6, Canada; Department of Construction Engineering, École de technologie supérieure, Montréal, QC H3C 1K3, Canada.
A. Ellery. Department of Mechanical and Aerospace Engineering, Carleton University, Ottawa, ON K1S 5B6, Canada.
Corresponding author: Claire Samson (e-mail: claire.samson@etsmtl.ca).

Introduction

The magnetic method is a widely used geophysical surveying technique used to map broad geological trends, detect ore bodies, or locate discrete magnetic sources. It is applied at different scales from large national territories to small prospective mining properties. To meet these different demands, magnetometers are deployed from a variety of platforms; they can be mounted on manned helicopters and fixed-wing aircraft for airborne operations, towed behind ships, carried by ground crews, and, more recently, used remotely with the development of unmanned aerial vehicles (UAVs) (Wood et al. 2016; Cunningham et al. 2017; Malehmir et al. 2017; Parvar et al. 2018). A new generation of lightweight magnetometers has been designed to meet the needs of the emerging UAV market. A novel opportunity exists for the instrumentation of unmanned ground vehicles (UGVs) with UAV magnetometers for robotic surveying.

UGVs expand the range of geophysical surveys into environments that are less suited to traditional methods. Under remote or autonomous operation, a UGV can deliver geophysical sensors into hazardous or difficult to access environments, such as mine tailings (Olmedo and Lipsett 2016), underground tunnels, or the surface of distant planetary bodies. By removing human operators from the survey area, UGVs can address niche applications, reduce risk, and extend coverage. A niche application suited to UGVs is unexploded ordnance detection, characterization, and mapping. UGV systems instrumented with electromagnetic sensors have proven highly effective at locating conductive targets in the near subsurface (Grusy 2009; Khamis 2013). In the context of planetary exploration, Lunokhod 2 is the only UGV carrying a magnetometer that has executed a mapping mission on the surface of a distant planetary body, the Moon, as early as 1973 (Dolginov et al. 1976). The Mars 2020 rover will be the first to do so on Mars (Weiss et al. 2014).

To explore the potential of UGVs for mapping the near subsurface using the magnetic geophysical method for terrestrial applications, a commercial UGV, the Husky A200 robotic development platform from Clearpath Robotics, was instrumented with the recently developed GSMP 35U potassium vapour magnetometer from GEM Systems. The objectives of the study were (*i*) to determine the impact of the magnetic UGV components on sensor data quality, (*ii*) to integrate the magnetometer and UGV in a practical configuration, and (*iii*) to evaluate the capability of the instrumented UGV to perform magnetic geophysical surveys (Hay 2017). A key issue was the interference caused by the UGV platform itself on the magnetic data. To minimize interference, a mounted tower design was implemented to increase the distance between the magnetometer and the magnetically susceptible components of the UGV. The integrated UGV was used to perform two comparative robotic magnetic surveys while mapping cultural targets and regional variations of the magnetic field.

The project was essentially an integration exercise where the UGV and the magnetometer were used together without changing their intrinsic designs, with the goal of identifying and assessing the severity of problems that would need to be addressed in the future development of this system or similar systems. It complements detailed studies that focus on reducing the signature of specific components of unmanned vehicle systems used for magnetic surveying (e.g., Forrester et al. 2014; Sterligov and Cherkasov 2016; Tuck et al. 2018) and on off-road robotics (e.g., Qadi et al. 2015; McGary et al. 2018).

Instrumentation and hardware

Magnetometers

Total magnetic intensity (TMI) data were acquired in this study using a GSMP 35U potassium magnetometer (GEM Systems 2015) in mobile operation and a GSM-19 Overhauser magnetometer (GEM Systems 2008) deployed as a base station (Table 1).

Table 1. Magnetometer specifications.

Parameter	GSMP 35U	GSM-19
Type	Potassium vapour	Overhauser effect proton precession
Sensor mass	0.65 kg	1.00 kg
Electronic box mass	0.63 kg	2.10 kg
Sensor dimension	158 mm × 64 mm	177 mm × 75 mm
Electronic box dimensions	237 mm × 56 mm × 39 mm	223 mm × 69 mm × 240 mm
Sensitivity	0.0003 nT @ 1 Hz	0.22 nT / $\sqrt{Hz}$
Resolution	0.0001 nT	0.01 nT
Absolute accuracy	±0.05 nT	±0.10 nT
Dynamic range	15 000–120 000 nT	20 000–120 000 nT
Gradient tolerance	50 000 nT/m	<10 000 nT/m
Sampling frequency	10 Hz	0.33 Hz

Table 2. Husky A200 robotic development platform specifications.

Parameter	Value
Mass: magnetometer module (kg)	3.18
Mass: sensor tower (kg)	0.40
Mass: magnetic sensor (kg)	0.65
Mass: UGV Chassis (kg)	50.00
Total mass (kg)	54.23
Speed (m/s)	1.00
Battery power	24 V, 20 Ah

Both magnetometers are designed to measure the total magnetic field B as a scalar value (Kearey et al. 2002). The GSMP 35U potassium vapour magnetometer was selected for integration with the Husky UGV platform due to its low weight, reduced dimensions, high sensitivity, and rugged design. With a 10 Hz sampling frequency, this magnetometer was well suited to maintaining a high spatial resolution during survey operations. Because of the lower frequency of diurnal variations, the base station magnetometer's 0.33 Hz sampling frequency and ±0.10 nT accuracy were sufficient for monitoring the magnetic background and to determine the diurnal corrections to be applied to survey data.

Husky unmanned ground vehicle

The Husky A200 robotic development platform (Clearpath Robotics 2018) is an all-terrain UGV designed for rapid prototyping and research applications (Table 2). The platform features a rugged design, onboard power supply, aluminum mounting rails, and open-source robotic operating system. The robotic platform was selected for magnetic surveying because of its 1.0 m/s full speed, 75 kg payload mass, and slip-drive mobility system. Functionally, its slip-drive performs well in diverse terrain conditions with high-torque electric motors capable of pushing through the light brush, rocks, loose gravel slopes, mud, and flooded fields that were encountered in the field. The 75 kg payload budget of the UGV was sufficient to easily incorporate the mass of the potassium magnetometer, aluminum tower, and electronics modules with negligible impact on mobility performance. The instrumented UGV was deployed in survey configuration (Fig. 1).

Operations module

Command and control of both the magnetometer and UGV were accomplished using an operations module built into the cargo bay of the UGV (Table 3). This module comprised the magnetometer electronics box, data cables, lithium batteries, and a microcontroller.

Fig. 1. Photograph of the Husky A200 UGV in survey configuration. A field laptop was employed for troubleshooting and monitoring but was not integral to the operation of the system.

Table 3. Operations module specifications.

Parameter	Value
Mass: Li-battery packs (kg)	1.46
Mass: electronics box (kg)	0.70
Mass: microcontrollers (kg)	0.34
Mass: data cables and adapters (kg)	0.75
Mass: total (kg)	3.35
Microcontroller battery capacity	5 V, 2600 mAh
Magnetometer battery capacity	25.9 V, 4000 mAh

The robotic operating system was modified to operate on the embedded microcontroller's reduced resources and configured to enable teleoperation either by wireless connection or tethered USB joystick. A supplementary microcontroller was later implemented within the operations module to log magnetic data from the magnetometer electronics box and to wirelessly broadcast real-time data to the operator.

Sensor tower

A tower was built to mount the survey magnetometer at a vertical distance of 121 cm from the top of the chassis along the *z*-axis (vertical axis centered on the UGV). From preliminary testing, it was noted that vertical oscillations of the sensor would be magnified by the lack of UGV suspension if combined with the leverage of a long boom, an effect that was noted on other boom-mounted UGV systems (Phelps et al. 2014). This is why a tower was preferred over a boom to provide support and mitigate oscillations of the sensor during motion of the platform.

Fig. 2. Magnetic scanning equipment setup. Traverses by the scanning cart along the rail (hollow arrow) were reversed for each subsequent scan. The *x*-axis is parallel to the rail, the *y*-axis is oriented out of the page, and the *z*-axis is oriented vertically.

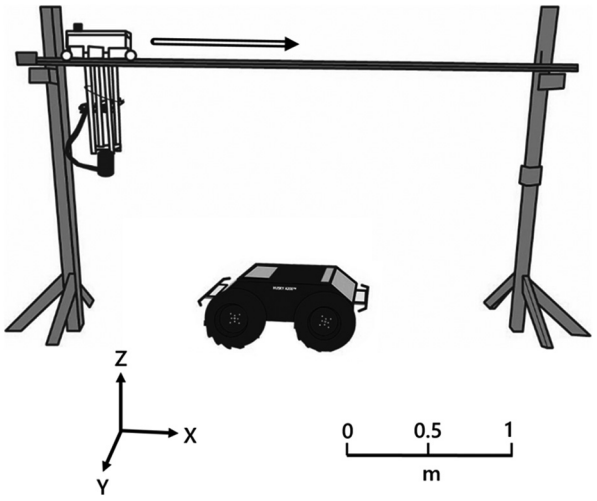

The tower was composed of a framework of vertical aluminum rails bolted to three horizontal frames using brass screws to form a semi-rigid lattice structure. Cross braces and bands of duct tape were applied to the vertical rails to make the structure more stable and more rigid, thereby damping the vibrations generated by UGV motion.

The base of the tower was secured to the UGV with four thumb screws bolted to the chassis' aluminum mounting rails. The survey magnetometer was mounted atop the tower in a vertical orientation and affixed with hook-and-loop straps, cable ties, and electrical tape. The elevation of the magnetic sensor was 160 cm relative to ground level when mounted to the UGV, a height comparable to that used by ground survey crews.

Robotic magnetic signature

Magnetic mapping of the unmanned ground vehicle

The chassis, mounting rails, bumpers, and plating of the UGV are composed of lightweight aluminum, which has a low magnetic susceptibility ($\sim 2 \times 10^{-5}$ SI units). Components containing ferrous materials included the wheel rims, axles, and electric motors. These components have a high magnetic susceptibility and are not ideal for robotic magnetic surveying. Tests were therefore performed in a laboratory setting to measure the influence of UGV components on the magnetic sensor. Magnetic scans were performed to identify regions of elevated magnetic intensity generated by the UGV platform at various orientations and distances from the survey magnetometer. A rail-mounted GSMP 35U magnetometer was used to measure TMI along the length of the chassis (*x*-axis) at a vertical separation distance of 33 cm above the UGV chassis (*z*-axis) for a series of traverses spanning the width of the UGV (*y*-axis) (Fig. 2). The UGV would then be repositioned with the same orientation, and a 10 cm incremental offset in the *y*-direction before the scanner would again traverse the rail. Data acquisition along each traverse generated a 1D magnetic profile of the UGV. The series of profiles were corrected for diurnal variation. The background (no UGV present) was subtracted from the data, which were then input to a Delaunay triangulation (Lee and Schachter 1980). In this fashion, two 110 cm × 200 cm 2D scanned maps of the TMI including the effects of the UGV were constructed.

Fig. 3. TMI map of the UGV with electric motors: (*a*) disconnected from the onboard battery power and (*b*) connected to onboard battery power at 0% throttle (idle). The position of the Husky UGV is outlined in black. Note that the TMI scale is different by one order of magnitude between the two maps.

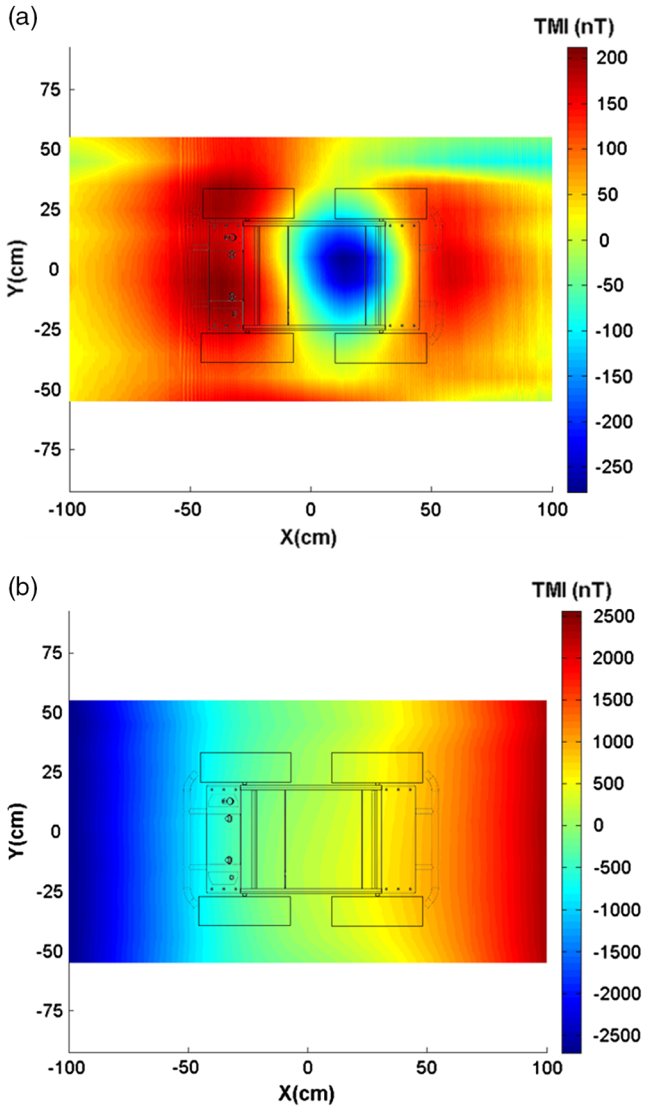

The first scan was undertaken while the UGV was powered with the electric motors disconnected from the onboard battery power using an emergency-stop switch (Fig. 3*a*). It shows a positive 200 nT magnetic response above the front and rear axles, and a 250 nT negative magnetic response centered on the UGV cargo bay. The second scan was undertaken with the electric motors reconnected to the onboard battery power at 0% throttle (Fig. 3*b*). A 2500 nT signal is readily apparent in the corresponding magnetic map with minor fluctuations being noted above the UGV axle positions. This sizable magnetic field has been attributed to the two electric motors, which were mounted to the chassis perpendicular to the axles.

Table 4. Amplitude and fourth difference of magnetic oscillations generated by the chassis wheels at different magnetometer–UGV separation distances.

Separation distance (cm)	Amplitude (nT)	Fourth difference (nT)
41	43.05	±1.37
60	30.56	±0.59
89	15.22	±0.28
105	10.58	±0.23
121	6.05	±0.17
150	2.23	±0.03
200	0.42	±0.02

Magnetometer–vehicle separation tests

TMI decreases at a rate of $1/r^3$, where r is the distance between the magnetometer and the magnetic source. To inform the choice of the height of the sensor tower, tests were conducted to assess the level of noise associated with the UGV chassis wheels, which are composed of steel rims with rubber tires and attached to steel axles by aluminum brackets and screws. During rotation of the chassis wheels, the TMI was recorded over a period of 20 s at several separation distances between the UGV chassis and the survey magnetometer (Table 4). Based on the results of these tests, a distance of 121 cm, corresponding to an oscillation amplitude of ±6.05 nT, was selected for the tower design as a compromise between noise reduction and mechanical practicality. To further reduce the amplitude by a factor of two, the distance would have to be increased to almost 150 cm, which may have caused the tower to become unstable. The selected distance of 121 cm is also the same as was used for the Kapvik rover (see section entitled "Carleton University campus robotic magnetic survey"), which facilitates comparisons.

To guide future design changes, a related test was performed at a separation distance of 121 cm without the steel wheel rims in place to isolate the impact of the rotation of the rims on the amplitude of magnetic oscillations. A notable 87% reduction was observed between the average oscillation amplitude before (6.05 nT) and after (0.79 nT) removing the steel wheel rims. The use of rims made of a magnetically inert material would be a simple solution to reduce the magnetic signature of the UGV in future applications.

Fourth difference analysis

To add a different perspective to noise analysis, the fourth difference was selected as a metric to evaluate the level of magnetic noise. The fourth difference at sample time (ΔT_0) is defined as

$$\frac{\Delta T_{-2} - 4\Delta T_{-1} + 6\Delta T_{o} - 4\Delta T_{+1} + \Delta T_{+2}}{16} \quad (1)$$

where ΔT_{-2}, ΔT_{-1}, ΔT_{+1}, and ΔT_{+2} are four values of the TMI sampled symmetrically with respect to, ΔT_0. An acceptable noise limit for the fourth difference is ±0.05 nT for commercial airborne surveys (Teskey et al. 1991; Coyle et al. 2014).

Fourth difference profiles were generated from all laboratory and field datasets to determine which factors would result in an increase in magnetic noise levels. The factors that were evaluated included magnetometer–UGV separation, the effect of wheel rotation, and vibration and mechanical noise related to the velocity of the UGV during survey operations. Environmental noise from outside sources, such as cultural noise from passing vehicles, was difficult to control and could only be mitigated by conducting tests and surveys during less active hours.

Table 5. UGV wheel rotation parameters.

Electric throttle (%)	Fundamental frequency (Hz)	Fundamental period (s)	UGV survey speed (m/s)
40	0.38	2.63	0.4
100	0.97	1.03	1.0

The fourth difference determined from magnetometer-separation test data confirms that increased separation distance greatly reduces noise (Table 4). With the sensor positioned at a distance of 41 cm from the UGV, the fourth difference is ±1.37 nT. As the sensor is positioned at a greater distance from the UGV chassis, the fourth difference is rapidly reduced by 80% to ±0.28 nT at 89 cm, and by 88% to ±0.17 nT at the selected separation of 121 cm.

The fourth difference was also used to investigate in detail the impact of wheel rotation on noise. The rotation period of the chassis wheels is manually controlled in increments of 10% throttle via the tethered joystick. The wheels of the UGV rotate with a period of approximately 2.63 s while at an electronically limited 40% throttle; this setting corresponds to the half-speed of 0.4 m/s. The pilot can manually override the throttle limiter with an electronic switch to decrease the rotation period of the wheels to approximately 1.03 s when the electric motors are at 100% throttle. The UGV then travels at a full-speed of 1.0 m/s. At a magnetometer–UGV separation distance of 121 cm, the fourth difference was ±0.10 nT during full-speed rotation of the steel wheel rims and axles. With the steel wheels removed, the fourth difference was ±0.07 nT, corresponding to a 30% decrease. The speed at which the wheels were rotating was also found to have a significant effect on the fourth difference. It was on average ±0.17 and ±0.11 nT when rims and axles were rotating at full and half-speed, respectively. At half-speed, because the wheels only complete half a rotation per second, the fourth difference, which uses five sequential readings spaced by 0.1 s in time for a total duration of 0.5 s, only captures a portion of the wheel rotation.

Spectral analysis

Fourier spectral analysis was used to determine the magnetic signature of the UGV in the frequency domain. Time series of 501 sequential data points sampled at 10 Hz were extracted from TMI laboratory datasets, normalized, corrected to remove linear trending, and then used as inputs in a fast Fourier transform algorithm to generate frequency spectra. The oscillations generated by the rotation of the steel wheel rims and axles have distinct spectral responses according to their periodicity (Table 5). Figure 4*a* displays the spectrum generated by the wheels rotating at 40% throttle. The fundamental spectral peak is at 0.38 Hz (corresponding to a period of 2.63 s for the wheel rotations), and the first harmonic peak is at 0.78 Hz. The spectrum generated when the steel wheels are removed also shows a peak at 0.38 Hz although at 9 dB lower maximum amplitude. The same trend is observed in the spectrum generated by the wheels rotating at full-speed with 100% throttle (Fig. 4*b*). The fundamental spectral peak is at 0.97 Hz (corresponding to a period of approximately 1.03 s for the wheel rotations) and the first harmonic peak at 1.94 Hz. There is a similar amplitude reduction of 9 dB when the steel wheel rims are removed.

Carleton University campus robotic magnetic survey

Survey site

The survey site, located on the campus of Carleton University, consisted of a rectangular 45 m × 12 m grid centered 40 m southeast of Herzberg Laboratories and 25 m southwest of Richcraft Hall (Fig. 5). Local infrastructure consisted of a buried storm sewer and a gas

Fig. 4. Frequency spectra of TMI time series when wheel rims are attached (blue) or removed (red) from axles, for rotation speeds of (*a*) 0.4 m/s and (*b*) 1.0 m/s. The spectral response of the ambient background in the laboratory is also plotted for reference (black).

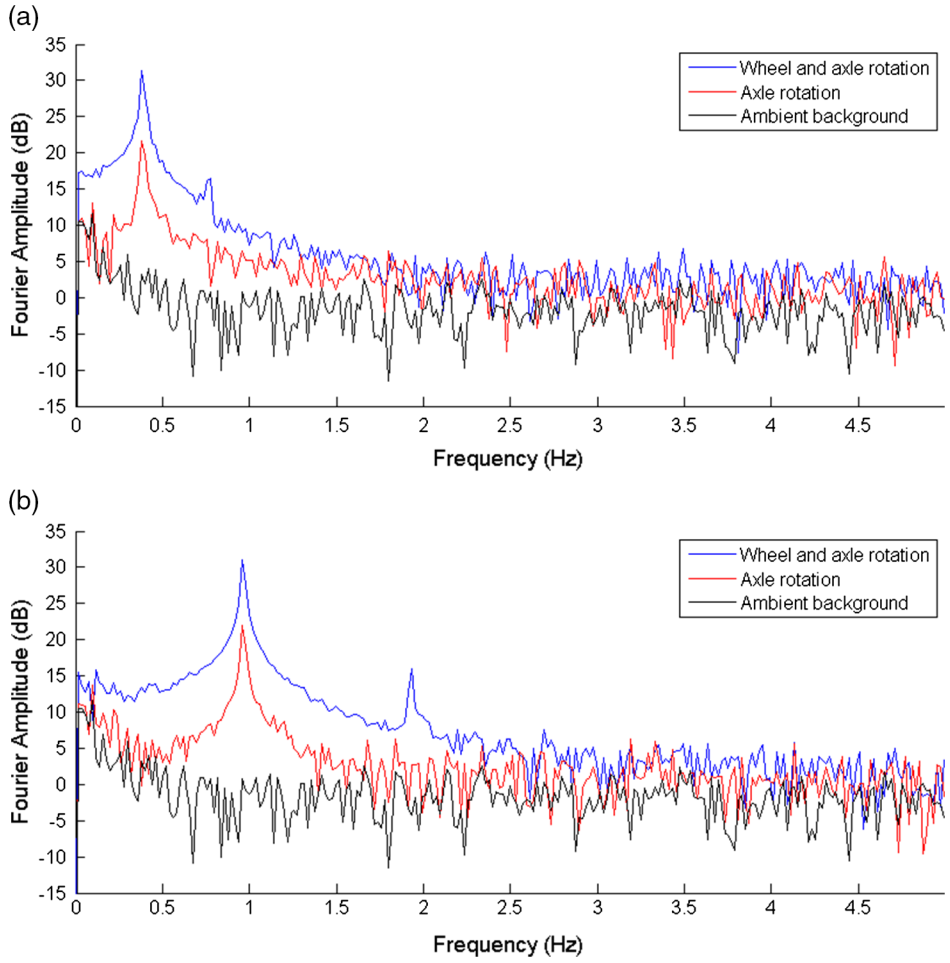

pipeline, surface walking paths traversing the middle of the grid, and an adjacent roadway. A light rail line is located 100 m east of the grid.

The grid layout consisted of five 45 m long survey profile lines at a 3 m line spacing oriented east–west with respect to magnetic north. Two 12 m long tie lines at the profile line end-points were oriented north–south. Profile line distances were measured manually using a fiberglass tape, and line end points were marked with pylons for use as navigational aids.

Data acquisition

The survey was conducted during weekday daylight hours. Mitigation of cultural noise sources was accomplished by waiting for local traffic patterns to slow before rapidly completing each line segment. This strategy took advantage of the fact that, at an operational speed of 1.0 m/s, the UGV only took approximately 45 s to cover a profile line. TMI data were recorded at a 10 Hz sampling frequency and recorded by the magnetometer in ASCII format. The spatial resolution of the UGV surveying at a relatively constant velocity of 1.0 m/s with a magnetometer sampling rate of 10 Hz is approximately 0.1 m. The UGV was tele-operated by

Fig. 5. Carleton campus survey grid. The positions of the profile (L 0N, L 3N, L 6N, and L 12N) and tie (T 0E and T 45E) lines (white), a subsurface storm sewer (purple), and a gas pipeline (yellow) are marked. Gridlines were oriented with respect to magnetic north (MN) at 13.3° W declination from the orientation of geographical north (star). Background image source: Google Earth.

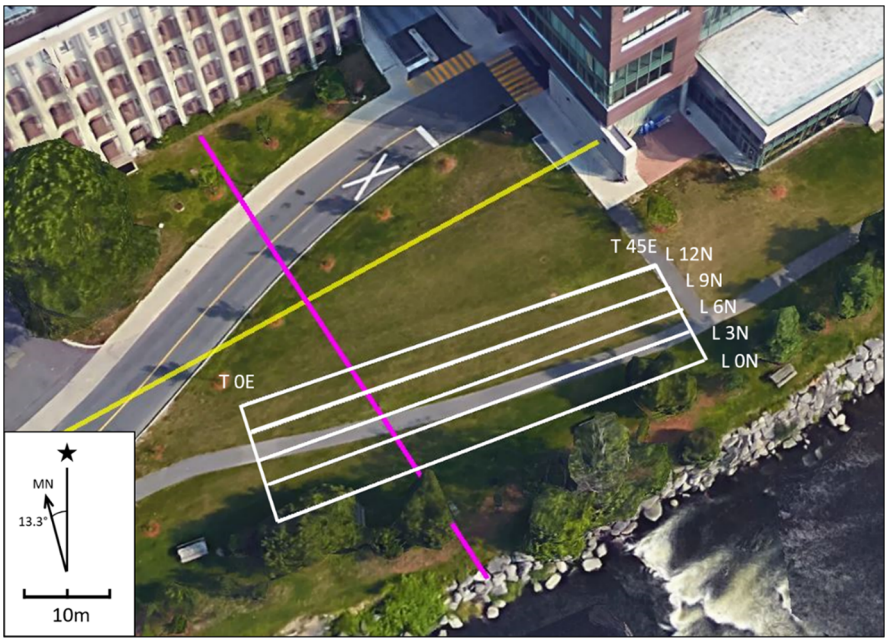

a human pilot tethered by USB joystick, following at a distance of 2 m. All recording equipments were manually synchronized to coordinated universal time (UTC) prior to the survey, and each data point was timestamped so that datasets could be stitched together in post-processing.

Data processing

The initial TMI dataset acquired by the UGV was diurnally corrected using data recorded at the Ottawa Geomagnetic Laboratory, a magnetic observatory located 11.5 km east of the survey site. The observatory data were generated at a 1 Hz sampling frequency, which resulted in the diurnal correction algorithm correcting asynchronous data points with linearly interpolated values. The diurnally corrected data were geolocated by stitching the corresponding GPS coordinates to each data point based upon a common UTC timestamp. The TMI for each of the profile lines was then levelled by linear interpolation using tie-line intercept values and normalized by removal of the ambient regional magnetic field intensity of 52 500 nT (see the example of line L 3N in Fig. 6). A 41 nT/m local trend, decreasing towards geographic north, was also removed from the dataset. This gradient was due, in large part, to infrastructure present adjacent to the survey grid (buildings and roadways).

Interpretation and discussion

The residual magnetic intensity scatter plot (Fig. 7) reveals a linear anomaly trending parallel to magnetic north. This feature has a maximum amplitude of 625 nT at location (−2 and −5 m), which corresponds to the known position of a subsurface storm sewer.

The fourth difference was calculated for each line segment. Figure 8 displays an example from line L 3N for the UGV during active survey operations at a velocity of 1.0 m/s.

Fig. 6. Post-processed TMI profile for line L 3N. Sinusoidal oscillations in the data are mainly attributed to the rotation of the UGV wheels.

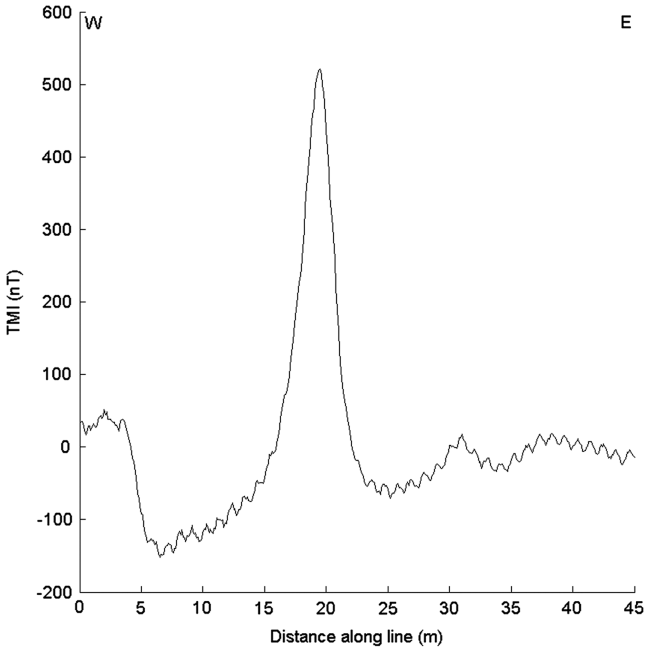

Fig. 7. Residual TMI scatterplot of the Carleton campus survey grid.

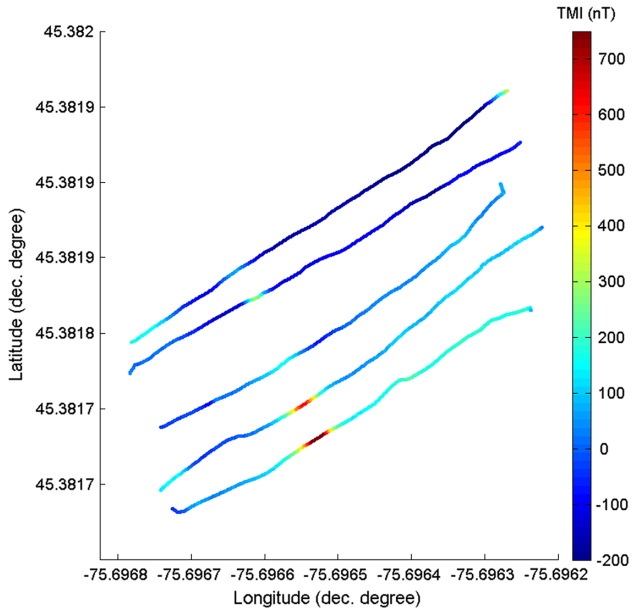

During line traverses, the fourth difference was ±1.97 nT, notably higher than the ±0.1 nT fourth difference observed during the wheel rotation tests for a speed of 1.0 m/s in the laboratory (Fig. 4*b*). The increased noise level is attributed to vibrations generated by the

Fig. 8. Fourth difference profile for line L 3N. The noise level is displayed as black dashed lines.

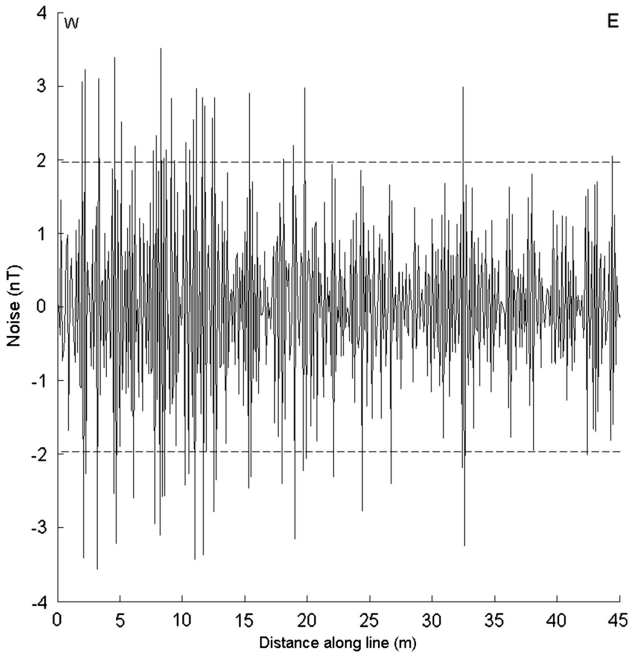

Table 6. Comparative results between robotic magnetic surveys at the Carleton University survey site (Fig. 11).

Parameter	Kapvik micro-rover	Husky UGV
Survey speed (m/s)	0.02	1.00
Surveyed distance (line m)	135	249
Spatial resolution (m)	0.002	0.1
Survey duration (min)	225	15
Productivity (line m/h)	36	996
Magnetometer–UGV separation (cm)	121	121
Maximum TMI recorded (nT)	418	522
Minimum TMI recorded (nT)	−336	−152
Fourth difference (std dev) (nT)	0.03	1.97

mechanical interaction of the ground with the wheels and geological magnetic noise from small disseminated sources.

A previous robotic magnetic survey was completed with the Kapvik micro-rover at the same location (Hay et al. 2017). The results generated by the two surveys are summarized in Table 6. The TMI ranges are 754 nT for the Kapvik micro-rover and 673 nT for the Husky UGV. The 650 nT anomalous linear response attributed to a buried storm sewer by the Kapvik micro-rover was detected at the same position by the Husky UGV at 625 nT, although at a much lower spatial resolution. During survey operations, the primary active component on each UGV was the rotation of the chassis wheels. On the Husky UGV, the wheels were found to generate much higher magnetic interference due to the combination of their ferromagnetic composition of the wheels and higher rotation speed (the survey speed achieved by the Husky UGV was 50 times faster than that of the Kapvik micro-rover). Consequently, the fourth difference was two orders of magnitude greater for the Husky

Table 7. Comparative results between UGV and human walking magnetic surveys at the Hay Bay survey site.

		Husky UGV	
Parameter	Walking	Full-speed	Half-speed
Survey speed (m/s)	1.1	1.0	0.4
Surveyed distance (production m)	2531	1679	1237
Survey duration (min)	50	38	50
Productivity (line m/h)	3037	2651	1484
Spatial resolution (m)	0.11	0.10	0.04
Magnetometer–vehicle separation (cm)	NA	121	121
Magnetometer height (cm)	160	160	160
Maximum TMI recorded (nT)	57 810	53 640	53 990
Minimum TMI recorded (nT)	51 330	51 910	52 641

UGV than for the Kapvik micro-rover. For the identification of relatively large near-surface cultural targets, the Husky UGV was sufficient to the task; with a productivity nearing 1000 m/h it was also a more practical choice.

Hay Bay robotic magnetic survey

Data acquisition

A robotic magnetic survey was conducted with the Husky UGV, in parallel with a human-operated walking survey, in the rural township of Greater Napanee, Ontario, Canada, to allow a comparison between both datasets (Table 7).

An initial survey of the site was conducted on 26 March 2016, by walking the GSMP 35U magnetometer mounted on a pole of 160 cm height while recording the TMI at a 10 Hz sampling frequency. A handheld GPS unit was employed to track the position of the operator and to help navigate by maintaining an east–west heading. UTC timing was used to synchronize the timestamps between the survey magnetometer, base station magnetometer, and GPS unit. Pylons were used as navigational references to guide the path of the operator. A follow-up survey of the same site was completed on 26 April 2016 with the Husky UGV following a similar path selection strategy. The UGV was tele-operated by a human pilot using a USB joystick and following at a distance of 2 m. The UGV survey was repeated twice, at full (1.0 m/s) and half-speed (0.4 m/s).

Data processing

Data for the diurnal correction were obtained from a base station magnetometer located within a magnetically quiet area of the survey site, where the local gradient was less than 1 nT/m. The diurnally corrected TMI dataset was then stitched with the timestamped GPS coordinates for geolocation. Segments of the dataset were cut where signal was weak or where a magnetic signal lock had been lost. The latter happened close to cultural sources. Because the datasets were gathered on different days, a static shift was applied to normalize the average TMI.

A subset of the data, acquired over flat terrain, is presented as scatter plots in Fig. 9. A 100 m long portion of the northernmost line was surveyed with the three methods to serve as a common reference line for comparison (Fig. 9). Figure 10 displays TMI and corresponding fourth difference profiles from the common reference line. Time series of 501 sequential data points from the common reference line were also used to determine the frequency content of the magnetic signal using a fast Fourier transform (Fig. 11).

Fig. 9. TMI scatter plots of the Hay Bay survey site. (*a*) Walking survey, (*b*) UGV survey at a velocity of 1.0 m/s. The white box indicates the location of the common reference line.

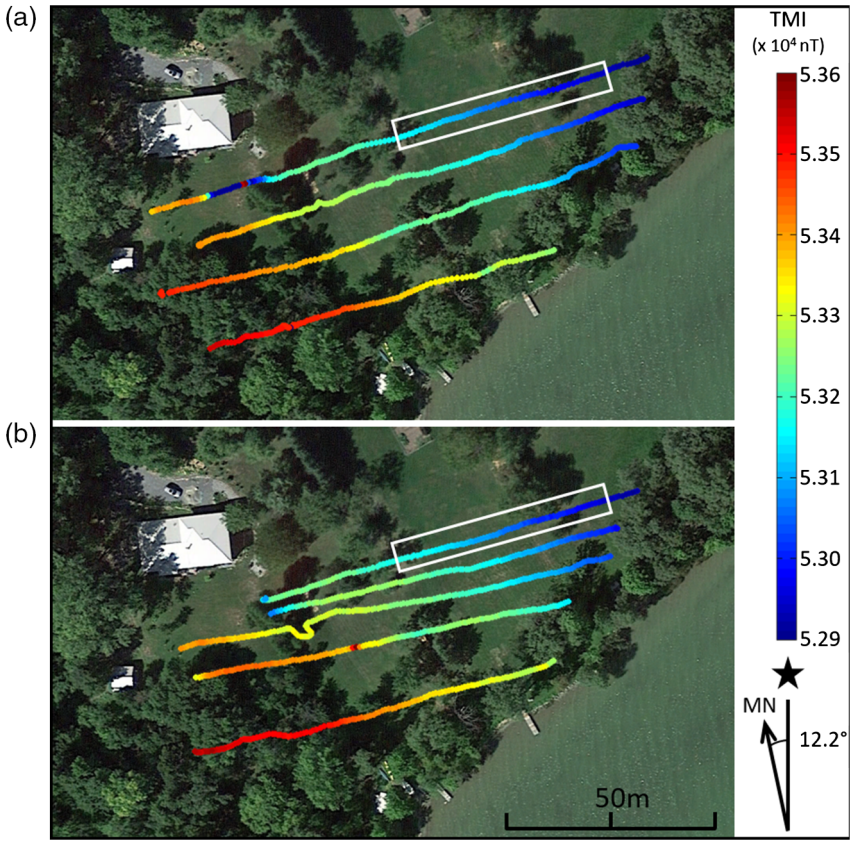

Interpretation and discussion

The scatter plots generated during the walking survey and the combined UGV survey (Fig. 9) show similar characteristics. Both scatter plots show a local gradient of 3.15 nT/m increasing to the southwest, with a few anomalous responses centered on cultural sources (residential homes, outbuildings, and farming equipment). The slight blurring at the transitions between magnetic levels from one colour to the next is a result of the magnetic oscillations generated by the UGV wheels as it travels (Fig. 9*b*). This artifact may prove detrimental to determining the accurate position of magnetic boundaries and anomalous responses.

The fourth difference was approximately ±0.1 nT for the walking survey, ±0.6 nT for the UGV at half-speed, and ±4.0 nT for the UGV at full speed (Fig. 10). In first approximation, the fourth difference increased by one order of magnitude between the walking survey and the half-speed UGV survey, and by another order of magnitude between the half and full-speed UGV surveys.

During survey operations, it was noted that the UGV operating at full speed was subject to significantly more vibration and shaking of the aluminum sensor tower than while travelling at half-speed. The mechanical forces acting upon the UGV and sensor are, in large part, due to a lack of suspension which, at low speeds, is not as severe as the rubber wheels are able to absorb the lesser shock at the ground–wheel interface. The frequency responses

Fig. 10. Comparison between TMI (left) and fourth difference profiles (right) for three survey modes. (*a*, *b*) Human operated, (*c*, *d*) Husky UGV operated at 0.4 m/s and (*e*, *f*) 1.0 m/s.

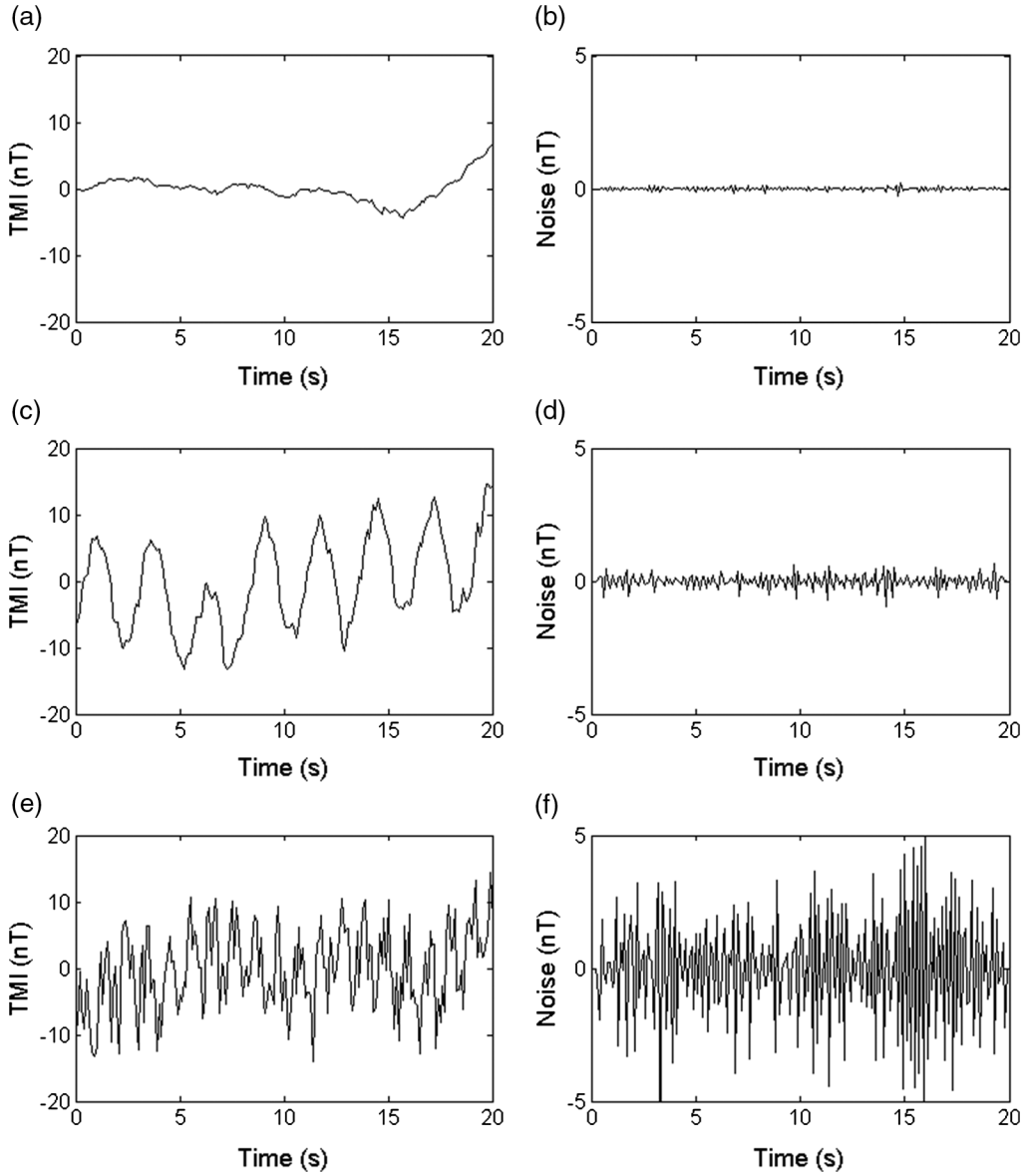

of the Husky during survey operations (Fig. 11) were different than those measured in controlled laboratory conditions (Fig. 4). The spectra generated at 0.4 and 1.0 m/s display spikes related to the periodicity of the steel wheels as they rotate. The field data, however, also show an increased magnitude across the entire frequency range but especially between 2 and 5 Hz. As previously noted, the UGV travelling at full speed was noted to experience higher mechanical forces acting upon the tower and sensor, which corresponds to a 7–10 dB magnitude increase between 2 and 5 Hz, compared with when travelling at the slower 0.4 m/s speed. For comparison, the walking survey frequency spectrum showed a magnitude

Fig. 11. Frequency spectra of TMI time series from the common reference line.

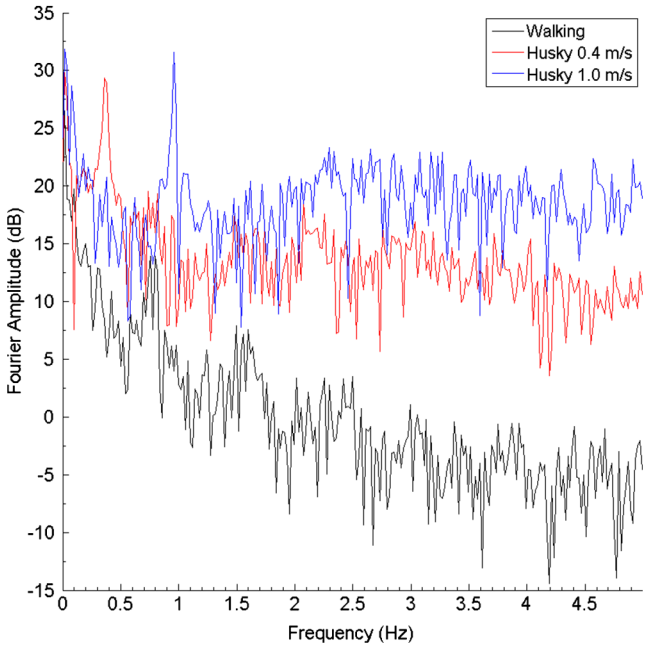

of 15 dB less over the 2–5 Hz range. During the walking survey, the sensor was subjected to reduced mechanical vibrations and oscillations because of the natural suspension of the human operator progressing at a steady gait.

Concluding remarks

The Husky UGV was designed for rapid scientific prototyping applications. When applied to magnetic surveying, it was found to have a large magnetic signature associated with ferromagnetic components in the electric motors and drive train. In laboratory conditions, during magnetic mapping of the static UGV powered on and with its wheel lockout disengaged, a variation of 5149 nT in TMI was observed over 2 m along the *x*-axis of the UGV at a height of 33 cm (Fig. 3*b*). In field survey conditions, the recorded TMI data were subject to oscillations of ±7 nT during active rotation of the chassis wheels, with a corresponding fourth difference of up to ±3.94 nT.

Testing the integrated UGV–magnetometer system has identified two hardware improvements that can be made to reduce the impact of ferromagnetic UGV components on the magnetic signal. The first improvement should be replacement of the ferromagnetic steel wheel rims with a nonmagnetic composite, aluminum, or plastic alternative, which would reduce the amplitude of magnetic oscillations by 84%. This modification would have the greatest impact on signal quality and would be simple to implement at a low cost. The second recommended improvement is a redesign of the sensor tower using a rigid composite. A rigid tower would be capable of supporting an increased sensor separation distance of 150 cm or higher while a customized composite could mitigate mechanical vibrations transmitted to the sensor. Further attenuation of magnetic noise could be achieved by applying a compensation to the data in post-processing, as is common practice in airborne geomagnetic surveying (Leliak 1961; Groom et al. 2004). Detailed compensation strategies could also be developed to track individual wheel odometry, position and

orientation of magnetic components, and used to compensate for variations in TMI due to orientation of the wheel, axles, and electric motors during survey operations (Forrester 2011; Forrester et al. 2014). Alternately, simpler signal processing strategies, such as applying a notch filter, a moving average filter (Versteeg et al. 2007) or a Hilbert transform (Green and Stanley 1975) could be applied to attenuate coherent noise in the magnetic signal.

The UGV was successfully integrated with the GSMP 35U magnetometer with the design and application of an aluminum sensor tower 121 cm in height. The sensor tower was able to mitigate 87% of the interference generated by the UGV systems at this separation distance. The integrated system was reliable during field surveys and generated magnetic datasets at a sampling frequency of 10 Hz and a spatial resolution of 0.1 m or better. The integrated UGV was initially deployed on a small survey in flat terrain on the Carleton University campus. During that initial survey, the position of a known cultural target was successfully identified by the detection of a magnetic anomaly generating a 625 nT response, and was consistent with results from a previous survey completed with the Kapvik micro-rover. A following survey at Hay Bay, Ontario, was also successfully completed, which demonstrated a robust system operation in realistic field conditions. While operating at a full speed of 1.0 m/s, the robotic UGV system production was found to be comparable with the productivity of a human walking survey.

With baseline results acquired for the Husky UGV instrumented with a magnetometer, there are opportunities to expand the applications of this integrated robotic system in the near future. One factor that limits current operations is the lack of remote operation capabilities. By integrating navigational sensors, such as a panoramic video camera and a radio communications relay, the UGV could be remotely piloted by a human teleoperator from a distant base station. This would enable analogue missions in hazardous environments, such as mine tailings ponds, unexploded ordnance contaminated terrain, and regions of active volcanism. Alternately, the autonomous features of the UGV could be expanded to incorporate real-time TMI data into path planning for simultaneous localization and mapping (SLAM). This could enable a UGV equipped with a magnetometer to autonomously seek out regions with pre-defined magnetic parameters, follow magnetic gradients, or determine the position of subsurface magnetic features.

Acknowledgements

This research project was funded by a NSERC (Natural Science and Engineering Research Council of Canada) ENGAGE grant to CS, in collaboration with GEM Systems Inc. The authors would like to acknowledge the support and technical insight provided by Michael Cunningham, Blair Walker, Benoît St-Louis, Lorne McKee, and Christopher Brown.

References

Clearpath Robotics. 2018. Husky unmanned ground vehicle user manual, Rev. 1.1.3., 25 p.

Coyle, M., Dumont, R., Keating, P., Kiss, F., and Miles, W. 2014. Geological survey of Canada aeromagnetic surveys: design, quality assurance, and data dissemination. GSC Open file 7660.

Cunningham, M., Samson, C., Wood, A., and Cook, I. 2017. Aeromagnetic surveying with a rotary-wing unmanned aircraft system: a case study from a zinc deposit in Nash Creek, New Brunswick, Canada. Pure Appl. Geophys. **175**: 3145–3158. doi: 10.1017/s00024-017-1736-2.

Dolginov, S.S., Yerochenko, Y.G., Sharova, V.A., Vnuchkova, T.A., Vanyan, L.L., Okulessky, B.A., and Bazilevsky, A.T. 1976. Study of magnetic field, rock magnetization and lunar electrical conductivity in the Bay Le Monnier. Moon, **15**(1–2): 3–14. doi: 10.1007/BF00562468.

Forrester, R.W. 2011. Magnetic signature control strategies for an unmanned aircraft system. M.App. Sci. thesis, Carleton University, Ottawa, Ont.

Forrester, R., Huq, M.S., Ahmadi, M., and Straznicky, P.V. 2014. Magnetic signature attenuation of an unmanned aircraft system for aeromagnetic survey. IEEE/ASME Trans. Mechatron. **19**(4): 1436–1446. doi: 10.1109/TMECH.2013.2285224.

GEM Systems. 2008. GSM-19 v7.0 instruction manual, Release 7.4., 149 p.
GEM Systems. 2015. GEM systems GSMP-35 datasheet. http://www.gemsys.ca/wp-content/themes/gemsystems/pdf/GEM_UAV_Solutions-GSMP_35U.pdf?lbisphpreq=1.
Green, R., and Stanley, J.M. 1975. Application of a Hilbert transform method to the interpretation of surface-vehicle magnetic data. Geophys. Prospect. **23**(1): 18–27. doi: 10.1111/j.1365-2478.1975.tb00677.x.
Groom, R.W., Ruizhong, J., and Lo, B. 2004. Magnetic compensation of magnetic noises related to aircraft's maneuvers in airborne survey. 17th EEGS Symposium on the Application of Geophysics to Engineering and Environmental Problems: 101–108.
Grusy, J.W. 2009. Air Force Research Laboratory robotics technology demonstration range clearance of unexploded ordnance at Massachusetts Military Reservation. Report AFRL-RX-TY-TR-2009-4572.
Hay, A. 2017. Instrumentation and application of unmanned ground vehicles for magnetic surveying. M.Sc. thesis, Carleton University, Ottawa, Ont.
Hay, A., Samson, C., and Ellery, A. 2017. Robotic magnetic mapping with the Kapvik planetary micro-rover. Int. J. Astrobiol. **17**: 218–227. doi: 10.1017/S1473550417000209.
Kearey, P., Brooks, M., and Hill, I. 2002. An introduction to geophysical exploration. Blackwell Science, Hoboken, N.J.
Khamis, A. 2013. Minesweepers: towards a landmine-free Egypt, and outdoor humanitarian demining robotic competition. J. ERW Mine Action, **17**(1): Article 5.
Lee, D.T., and Schachter, B.J. 1980. Two algorithms for constructing a Delaunay triangulation. Int. J. Comput. Inf. Sci. **9**(3): 219–242. doi: 10.1007/BF00977785.
Leliak, P. 1961. Identification and evaluation of magnetic field sources of magnetic airborne detector equipped aircraft. IRE Trans. Aerosp. Navig. Electron. ANE, **8**(3): 95–105.
Malehmir, A., Dynesius, L., Paulusson, K., Paulusson, A., Johansson, H., Bastani, M., Wedmark, M., and Mardsen, P. 2017. The potential of rotary-wing UAV-based magnetic surveys for mineral exploration: a case study from central Sweden. Lead. Edge, **36**(7): 552–557. doi: 10.1190/tle36070552.1.
McGary, P., Yoon, D., Tang, T., Pomerleau, F., and Barfoot, T.D. 2018. Field deployment of the tethered robotic eXplorer to map extremely steep terrain. Proceedings of the 11th Field and Service Robotics Conference, Zurich, Switzerland.
Olmedo, N.A., and Lipsett, G.M. 2016. Design and field experimentation of a robotic system for tailings characterization. J. Unmanned Veh. Syst. **4**(3): 169–192. doi: 10.1139/juvs-2015-0034.
Qadi, A., Cloutis, E., Samson, C., Whyte, L., Ellery, A., Bell, J.F., Berard, G., Boivin, A., Haddad, E., Jamroz, W., Kruzelecky, R., Mack, A., Mann, P., Olsen, K., Perrot, M., Popa, D., Rhind, T., Sharma, R., Stromberg, J., Strong, K., Tremblay, A., Wilhem, R., Wing, B., and Wong, B. 2015. Mars methane analogue mission: mission simulation and rover operations at Jeffrey mine and Norbestos mine, Quebec, Canada. Adv. Space Res. **55**(10): 2414–2426. doi: 10.1016/j.asr.2014.12.008.
Parvar, K., Braun, A., Layton-Matthews, D., and Burns, M. 2018. UAV magnetometry for chromite exploration in the Samail ophiolite sequence, *Oman*. J. Unmanned Veh. Syst. **6**(1): 57–69. doi: 10.1139/juvs-2017-0015.
Phelps, G., Ippolito, C., Lee, R., Spritzer, J., and Yeh, Y. 2014. Investigations into near-real-time surveying for geophysical data collection using an autonomous ground vehicle. USGS Open File Report 2013–14. doi: 10.3133/ofr20141013.
Sterligov, B., and Cherkasov, S. 2016. Reducing magnetic noise of an unmanned aerial vehicle for high-quality magnetic surveys. Int. J. Geophys. **2016**: 7. doi: 10.1155/2016/4098275.
Teskey, D.J., Barlow, R., Hood, P.J., Lefebvre, D., Paterson, N., Reford, M., and Watson, D. 1991. Guide to aeromagnetic specifications and contracts. GSC Open File 2349.
Tuck, L., Samson, C., Laliberté, J., Wells, M., and Bélanger, F. 2018. Magnetic interference testing method for an electric fixed-wing unmanned aircraft system. J. Unmanned Veh. Syst. **6**(3): 177–194. doi: 10.1139/juvs-2018-0006.
Versteeg, R., McKay, M., Anderson, M., Johnson, R., Selfridge, B., and Bennett, J. 2007. Feasibility study for an autonomous UAV-magnetometer system. Idaho National Laboratory Report INL/EXT-07-13386.
Weiss, B.P., Russell, C.T., Anderson, B.J., Kirschvink, J.L., Golombek, M.P., Raymond, C.A., and Murphy, N. 2014. Mars Compass: a magnetometer for the Mars 2020 rover. 45th Lunar and Planetary Science Conference: abstract 2696.
Wood, A., Cook, I., Doyle, B., Cunningham, M, and Samson, C. 2016. Experimental aeromagnetic survey using an unmanned air system. Lead. Edge, **35**(3): 270–273. doi: 10.1190/tle35030270.1.